

Machine Vision Using Multi-Spectral Imaging for Undercarriage Inspection of Railroad Equipment

J.M. Hart, E. Resendiz, B. Freid, S. Sawadisavi, C.P.L. Barkan, N. Ahuja

University of Illinois at Urbana-Champaign, Urbana, USA

Abstract

Locomotive and rolling stock condition is an important element of railway safety, reliability, and service quality. Traditionally, railroads have monitored equipment condition by conducting regular inspections. Over the past several decades, certain inspection tasks have been automated using technologies that have reduced the cost and increased the effectiveness of the inspection. However, the inspection of most aspects of railroad equipment undercarriages is conducted manually. This is a labor-intensive process and often requires that railroad equipment be taken out of service so that the inspection can be conducted on specially equipped pit tracks. Machine vision technology offers the potential to quickly and automatically monitor, assess, record, and transmit detailed information regarding the condition of railroad equipment undercarriages and components. Multi-spectral imaging (e.g. visible and infrared range) allows recording of both physical and thermal condition and correlation between the two. This allows precise comparison of any undercarriage component or element of interest using templates, and/or references to previously recorded inspections, of the same or similar equipment and enables other analyses such as trending of component wear and detection of progressive increases in component heating over time. Multi-spectrum machine vision algorithms can determine if a component is outside its normal operating range and if anomalies are correlated across different spectra. The inspection tasks of particular interest for this investigation include disc brake condition, bearing performance, and detection of incipient failure of electrical systems such as locomotive traction motors and air conditioning units. We are also investigating detection of damaged or missing components and foreign objects.

Introduction

This paper describes research conducted to develop a new approach to undercarriage inspection using machine vision and multispectral imaging [1, 6]. This research was carried out by an interdisciplinary group of researchers working with experts in various other fields (studio lighting, infrared cameras and imaging, and passenger car inspection). Previous research by the University of Illinois at Urbana-Champaign on machine vision inspection systems provided a foundation for this project. These include recording digital video of trains passing by a fixed video camera [4, 7, 8] and the generation of panoramas of entire trains from these videos [8]. In this research we incorporated a below-track perspective and the integration of both visible and infrared spectrum images. Recording in-service trains at an operating passenger car service and inspection facility required consideration of various environmental factors and effects of adverse weather conditions. The specific inspection tasks we concentrated on were disc brake performance, bearing wear, locomotive traction motors, air-conditioning (A.C.) units and other electrical-based systems. These components are a source of thermal energy and certain incipient failures may be discovered through detection of irregularities or anomalies in their thermal signature. In combination with the visible spectrum images, their type and location can also be ascertained. In addition, the visible spectrum images can be used to detect damaged or missing components and foreign objects. These components and tasks formed the basis for our investigation of the feasibility of monitoring the health of rolling stock and locomotives using multi-spectral machine vision.

Approach

Our approach can be described in three basic modules consisting of: video acquisition, panoramic image generation, and machine vision inspection to identify foreign, missing, and damaged components (Figure 1). In the first module, visible and infrared (thermal) cameras were placed below the track and video recordings made of the train's undercarriage as it passed above. In Module 2, these videos were used to create continuous undercarriage panoramic images in both visible and thermal spectra for all the railcars and locomotives in the train. These train panoramas were split into single car panoramas using machine vision algorithms to first detect the location of the axles and then the couplers. In Module 3, these individual car panoramas were compared with unique templates representing specific car types in normal condition, and car-level anomalies such as missing or foreign components were detected. Integration of the thermal panoramas with the visible panoramas was used to isolate and identify components with thermal anomalies. In conjunction with car-level templates, more detailed templates of specific components of interest were also produced. These component-level templates can identify lower level defects associated with these specific components. Additionally, like components on the same car or in the same train are compared to find thermal outliers; such as brake discs whose simultaneous application should produce similar temperature increases. The methods for thermal and visible anomaly detection can be used to detect overheating components and possible incipient failure indicators so that they can be repaired before they manifest as physical damage or an in-service failure.

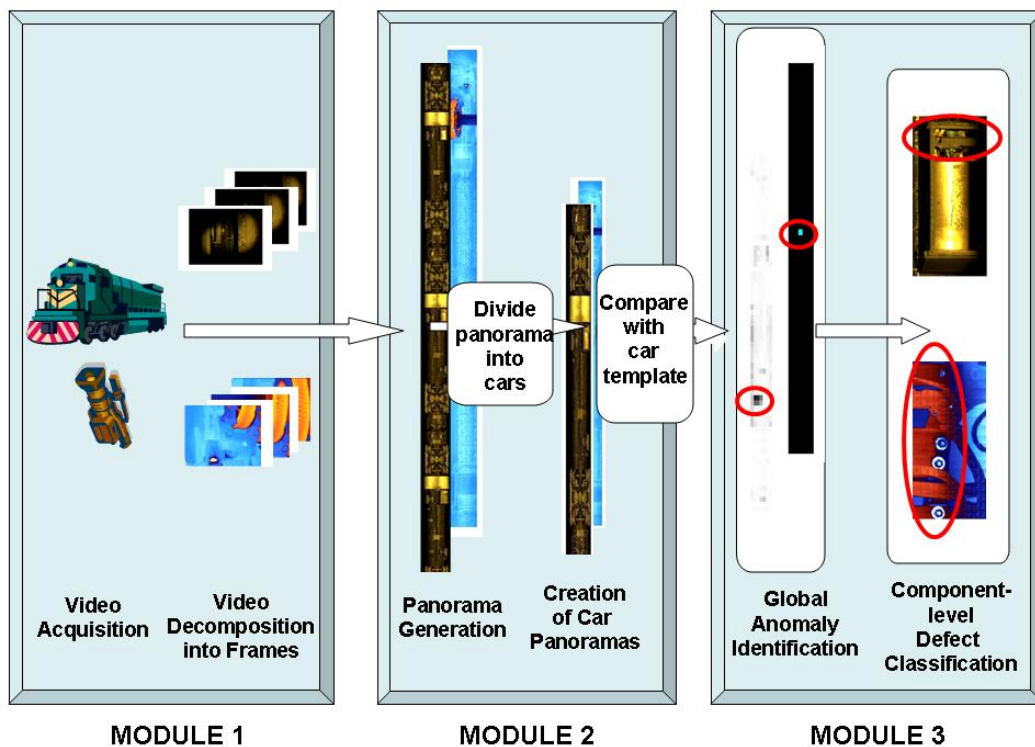


Figure 1: Overview of the multispectral inspection system.

Module 1: Image Acquisition and Pre-processing

Image Acquisition Prototype Development

Recordings were made with the camera mounted in an inspection pit, below rail level and looking upward at the bottom of the train (Figure 2). The factor limiting the camera's view of the entire undercarriage is the gauge face of the rail. We determined the focal properties required to provide the necessary field of view in terms of image width and height and from this, the maximum depth of the camera lens below the railhead for a given piece of rolling stock. For a

railcar with a maximum width of 10.5 feet and an undercarriage 50 inches above the railhead, the maximum depth (l) was calculated using Equation (1)

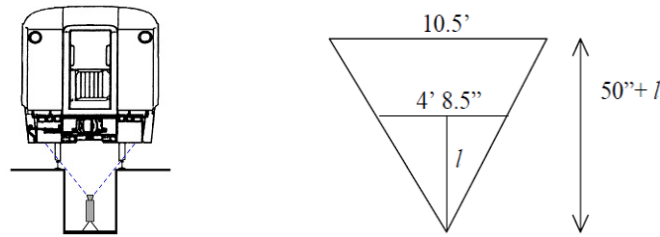


Figure 2: Camera perspective from beneath railcar and inverted triangle view.

$$\frac{50 + l}{126} = \frac{l}{56.5} \Rightarrow l = \frac{2825}{69.5} = 40.65'' = 3.39 \quad (1)$$

The video camera has two characteristics that determine the field of view: the camera's charge coupled device (CCD) size and the focal length of the lens. The camera we used has a $\frac{1}{2}$ inch CCD. Equation (2) is a general equation that relates focal length (f) with distance from the scene to the lens (D) and horizontal width (w). To calculate the appropriate focal length, we assumed a pit depth of 4 feet, and an enclosure slightly over 12 inches long and mounted on a tripod, giving a depth of 34 inches. Given that the horizontal width was 4 feet 8.5 inches at railhead height, and the constant (k) is 6.4 for a $\frac{1}{2}$ inch CCD, we calculated an optimal focal length of 3.9mm (Equation 2). A 3.9mm lens was not available but a 3.6mm lens was found to be satisfactory and was used instead.

$$f = k \frac{D}{w} = 6.4 \frac{34.00}{56.5} = 3.9mm \quad (2)$$

Similar considerations are needed for infrared imaging. Unfortunately, we were unable to obtain infrared camera lenses shorter than a 25mm lens, which is much longer than the 3.6mm lens used by the visible spectrum camera to capture the entire undercarriage. The 25mm lens did not allow the camera to capture the entire width of the undercarriage, so it was positioned to record a selected portion instead.

Undercarriage Lighting for Visible Spectrum Recordings

Based on initial experimentation and input from motion-picture lighting experts, we determined that four, studio-style 1,000-watt incandescent lights could provide adequate lighting (Figure 3a). In addition, we used scrims (light inhibiting screens) to achieve uniform illumination across the undercarriage. The gray half of each light in the diagram represents the scrim placement (Figure 3b). The relative uniformity of light intensity on the undercarriage was assessed using a light meter on a flat target held 50 inches above the railhead. The infrared camera was tilted 13-degrees toward the edge of the pit in order to minimize infrared backplane reflection and align the infrared viewable area with the components of interest.

We used a digital video camera that records 640x480-pixel resolution images (Figure 4a) at 30 frames per second. A laptop computer was used to control the visible spectrum camera via a FireWire connection long enough to allow the computer to be located outside the pit. The focus of the visible-range camera was adjusted using targets at a distance roughly equivalent to the location of the undercarriage. The same method was effective for focusing the infrared camera (Figure 4b).

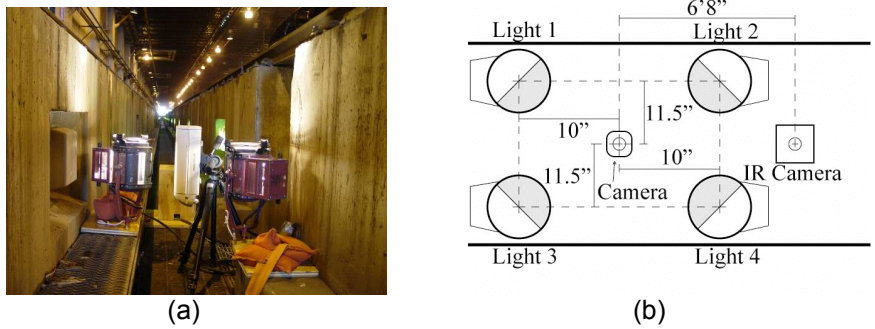


Figure 3: (a) Camera and lighting setup in Amtrak pit and (b) plan view of equipment setup.

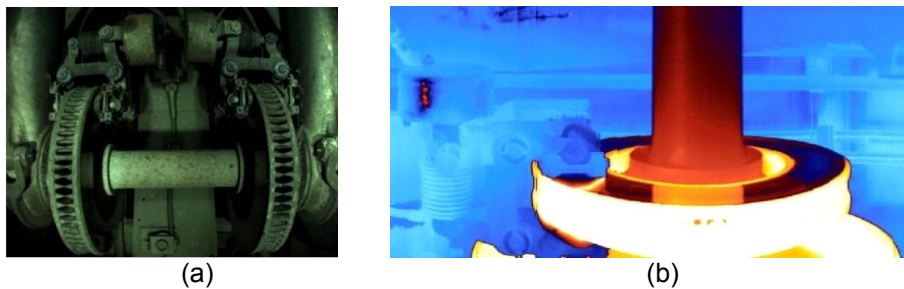


Figure 4: (a) Field-of-view of the visible image, and (b) thermal image; white pixels indicate a high brake drum temperature.

Both the A.C. unit and traction motor were located in the thermal and visible domains. The red area in Figure 5 indicates that the motor for the A.C. unit is hotter than its surroundings. The portion of the motor that is occluded by the rectangular covering in the visible domain becomes apparent in the thermal domain. The train speed was the normal pit speed of approximately 3mph; however, the system could be modified for faster train speeds by increasing the video frame rate and using a shutter speed fast enough to prevent motion blur. More powerful lighting and/or a more sensitive CCD would also be required to accommodate these changes. The infrared camera was sensitive to ambient temperature, and needed to be recalibrated with significant ambient temperature changes. A production system for this technology would require development of an automated method of infrared camera adjustment to achieve consistent clarity for different trains operating in different conditions.

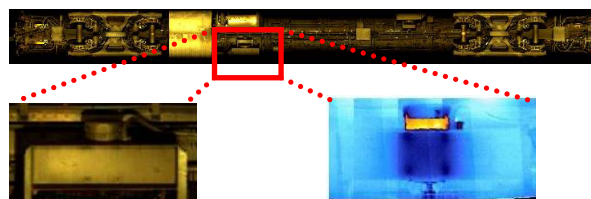


Figure 5: Visible and infrared images of air conditioning blower unit.

Module 2: Panoramic Image Processing

Panoramas were generated by stitching together center strips of consecutive frames where the height of each center strip was determined by the inter-frame displacement. This was determined by fixing one frame and shifting the following frame opposite the direction of train motion until a pixel displacement, d , is found that minimizes the sum of absolute difference (SAD) between the two frames. A center strip of height d from the first frame is stitched into the panorama. This allows the train to move at variable speeds and accounts for depth-induced velocity differences in the undercarriage. The thermal panorama is formed in the same way. The train's panorama is then parsed into individual car panoramas. Wheelset (wheel, axle, and brake disc) detection is used to approximate each car's length and location, followed by coupler

detection to detect car ends. Without axle detection, coupler detection is less robust since couplers have varied shapes and can be partially occluded. Axle detection is achieved by matching the edges of the panorama with the edges of an axle template, which are determined using a Canny edge detector [5]. Edges are used in matching because intensity variations are expected in both the visible and thermal images. A distance transform (DT) is used for robust matching since it doesn't require a one-to-one match between the one-pixel-width edges [2].

Relative to the visible-range camera, the infrared camera produced a magnified view due to its longer focal-length lens. To correct for this scale difference, the axle edge template was iteratively scaled to different sizes, and DT was used with the thermal edge image to find the best scale. Using the detected axles as anchor points, the thermal panorama was registered and overlaid with the visible panorama.

Module 3: Machine Vision Inspection

Global and coarse-level anomalies, in panoramas of both spectra, are detected in Module 3A. Then, individual components are inspected locally in Module 3B. Finally, components found at multiple locations in a railcar are analyzed to identify operational outliers in Module 3C.

Module 3A: Global Anomaly Detection

A relatively coarse-level analysis could be used for detection of foreign or missing components by comparing the railcar panorama to a car-level template. Car-specific visible and thermal templates were created and stored for each piece of equipment to allow for unique configurations due to repairs and other modifications. To detect anomalies, block-level correlation was performed between the recorded panorama (Figure 6b) and the railcar's template (Figure 6a). An example of anomaly detection is illustrated by the junction box present in the panorama for the car but not in the template. Areas of mismatch have a low correlation and the junction box is clearly evident (dark area in Figure 6c). Detection of thermal

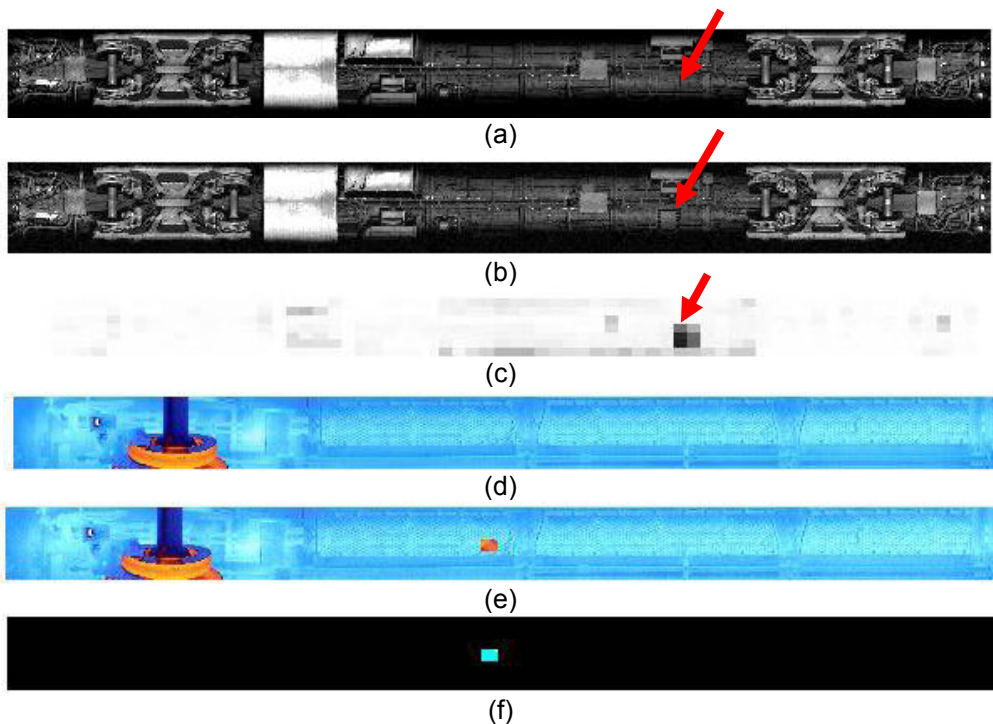


Figure 6: (a) Visible undercarriage template of an Amfleet-II coach, (b) undercarriage with an anomaly (a junction box not present on the template), and (c) the detected anomaly (dark block). (d) Partial thermal undercarriage template of an Amtrak Superliner car, (e) undercarriage with thermal anomaly, and (f) the detected anomaly (light blue block).

anomalies is computed in a similar manner using differences in color values between the thermal panorama and the car's thermal template (Figures 6d – 6f).

Module 3B: Component-level Anomaly Detection

Individual components were compared to the corresponding templates that contained the normal visible (or thermal) characteristics for each component. There should be one template for any allowable version of a component. The undercarriage components were examined in three steps.

Step 1: Align components with template

In the first step, we spatially aligned the components with their template using the DT applied to Canny edge images. An example is a template formed by merging three water tank images. The median-filtering technique was used to form a composite image (Figure 7a). A particular water tank, after alignment was compared to the template and its missing faceplate is evident (Figure 7b). The thermal components are similarly aligned with their templates and then registered with the corresponding visible images.

Step 2: Identify areas of mismatch

In the second step, the areas of dissimilarity between the template and the detected component are identified (Figure 7c). We created small windows around each pixel in both the visible and thermal images. In the visible domain, we computed the correlation between the template and the potentially defective component for each pixel window, and in the thermal domain, the luminance difference is computed. Anomalous pixels in the visible and thermal images are pixels whose surrounding windows have exceeded the correlation or luminance difference threshold, respectively. The areas of low correlation in the visible domain between the water container template and a defective component can be seen in Figure 7c. Thermally mismatched areas were also located.

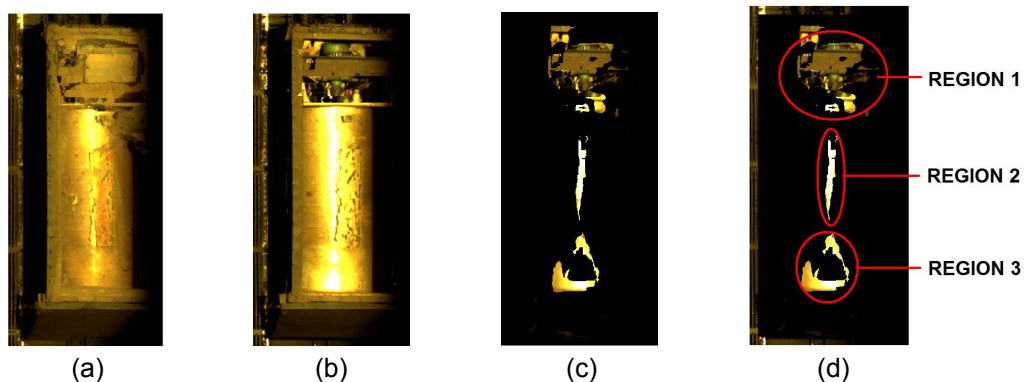


Figure 7: (a) Water tank template, (b) defective water tank, (c) areas of visible mismatch, and (d) areas of mismatch, grouped into regions.

Step 3: Learn defect categories

In the third step, the areas from Step 2 are grouped into contiguous regions of similar pixels using the K-means clustering algorithm [3]. The following features were extracted from each region: 1) (x,y) coordinates of the centroid; 2) the mean red, green, and blue color values; 3) region area in pixels; 4) simple shape estimation (eccentricity); and 5) a measure of how compact the boundary is (compactness). Thus, each anomalous region can be represented by a five-dimensional (5D) feature vector. Each defect category is represented in the 5D feature space using a Gaussian mixture model (GMM) [3]. In our GMM, a single anomaly category is represented by a weighted combination of several Gaussian probability distributions. We learn the weighting coefficients and Gaussian parameters by training on examples of anomalous regions.

Human intervention is required during training to classify regions. The class labels can be rough (defect/no defect) or specific (defect-corrosion, no defect-shine, defect-missing faceplate). In case an external condition causes a mismatch with the template (e.g., snow or ice buildup), it can be added as a class; therefore, this condition can be classified if encountered again. Regions from the thermal defective areas are learned similarly, and visible and thermal defects can be integrated in future work. In Figure 7d, the areas of mismatch have been grouped into regions and the classifications from training are shown. Two categories of regions were labeled by human intervention: “Missing Faceplate” and “No Defect – Shine”. Region 1 was labeled “Missing Faceplate” and Regions 2 and 3 were both labeled “No Defect – Shine”.

During testing, the GMM classifier is tested on previously unseen regions. We created a different segmentation from Figure 7c during testing in which Regions 2 and 3 from Figure 7d were combined into one large region. This larger region was classified correctly (shine). This demonstrates the generalization capability of a GMM for defect classification and its robustness to different region formation (segmentation) methods. Further, we can eliminate false positives by incorporating benign defect categories into the classification. Similar results were achieved using region-based grouping of anomalous temperature regions.

Module 3C: Relative Anomaly Detection of Like Components

Individual components that are found at several locations in an undercarriage are inspected for operational consistency. For example, a locomotive’s traction motors, a passenger car’s A.C. blower units, and a car’s brakes should all be operating uniformly.

The temperature of each brake disc was recorded, and temperatures that are anomalous with respect to other brakes were identified. In Table 1, brighter orange and higher luminance corresponds to a hotter disc brake. Without predefined operating ranges, we considered the hottest brake as an outlier (in Table 1, the luminance of Brake 1 of Car 2 is 1.5 times the standard deviation).

Using the edge image, the operating size of the return spring compression and the brake caliper are then measured to troubleshoot. This measurement indicates the contraction of the return spring device, and the resulting brake caliper contraction. This can then be used in a hybrid feature space that contains both distance and thermal measurements for further diagnosis. In Car 2, because of the smaller brake caliper opening and higher temperature of Brake 1, a thinner brake pad (with respect to Brake 2) is suspected. The diagnostic measurements along with the brake temperatures could also be learned using a GMM.

	Car 1		Car 2		Car 3		Car 4	
	Brake 1	Brake 2	Brake 1	Brake 2	Brake 1	Brake 2	Brake 1	Brake 2
Image of Disc Brake Area								
Mean Luminance	0.37	0.39	0.58	0.49	0.47	0.45	0.32	0.37

Table 1: Images of different car and axle brake thermal condition.

In our application, we have detected thermal outliers, and then used diagnostic measurements to form a course diagnosis (e.g. thin brake pads). Further knowledge of brake failure causes would be needed for a working system. With more data and domain knowledge, incorporating visible and thermal outlier identification followed by troubleshooting would be used to verify uniform component operation of the traction motors and A.C. blower units as well.

Conclusion

The work presented here demonstrates that multispectral machine vision offers substantial potential advantages to inspection and repair personnel for monitoring the health of railroad equipment. The creation of detailed, whole-train panoramic images and whole-car templates for comparison offers unprecedented inspection and condition monitoring capabilities for railway rolling stock and locomotive undercarriages. Using these images, the system can enhance normal visual inspections for missing or damaged components, and potentially identify foreign objects. The system has the additional advantage of facilitating digital recording and quantification of inspection results for comparison and trending. A significant additional benefit of the technology described in this paper is that the system provides a thermal view to help identify overheating or overworked mechanical and electrical components. Beyond this, we have demonstrated that through the integration of the visible and thermal views, diagnosis of incipient failures can be determined. We have also shown that the inherent cause of an incipient failure may be able to be isolated. Using multi-spectral machine vision techniques on railcar panoramas allows the system to monitor the physical and thermal condition of railroad equipment more efficiently and effectively than is possible using current methods and technologies.

Acknowledgements

This research was funded by the Transportation Research Board – High-Speed Rail IDEA Program, Project HSR-49. We are grateful to James Lundgren of the Transportation Technology Center, Inc. and Paul Steets, John Raila, and Dale Kay of Amtrak for their assistance, cooperation and guidance on this project. Thanks also to Gavin Horn for use of, and training on, the infrared camera, and to Derrick Hammer who provided the motion picture lighting equipment and guidance on its use. Special thanks to Amtrak and the Monticello Railway Museum for their cooperation and generous use of facilities.

References

- [1] N. Ahuja and C. Barkan, "Machine Vision for Railroad Equipment Undercarriage Inspection Using Multi-Spectral Imaging", *Transportation Research Board High-Speed Rail IDEA Program Final Report*, (2007).
- [2] H.G. Barrow, J.M. Tanenbaum, R.C. Botles and H.C. Wolf, "Parametric correspondence and chamfer matching: Two new techniques for image matching," In: *Proc. of 5th Int'l. Joint Conf. on Artificial Intelligence*, Cambridge, MA, pp. 659–653, (1977).
- [3] Bishop, C., *Pattern Recognition and Machine Learning*. New York: Springer, (2006).
- [4] J.R. Edwards, C.P.L. Barkan, J.M. Hart, S. Todorovic, N. Ahuja, "Improving the efficiency and effectiveness of railcar safety appliance inspection using machine vision technology". JRC2006-94052, In: *Proc. of the ASME JRC2006 Joint Rail Conf.*, Atlanta, GA, Apr. 4-6, (2006).
- [5] D.A. Forsyth, and J. Ponce, *Computer Vision: A Modern Approach*. Prentice Hall, (2003).
- [6] B. Freid, C.P.L. Barkan, N. Ahuja, J.M. Hart, S. Todorovic, N. Kocher, "Multispectral Machine Vision for Improved Undercarriage Inspection of Railroad Rolling Stock". In: *Proc. of the Int'l Heavy Haul Conf. "Specialist Technical Session"*, Kiruna, Sweden, pp. 737-744, (2007).
- [7] J.M. Hart, N. Ahuja, C.P.L. Barkan, D.D. Davis, "A Machine Vision System for Monitoring Railcar Health: Preliminary Results", *TD-04-008*, Association of American Railroads, (2004).
- [8] Y-C. Lai, C.P.L. Barkan, J. Drapa, N. Ahuja, J.M. Hart, P.J. Narayanan, C.V. Jawahar, A. Kumar, L. Milhon and M.P. Stehly. "Machine vision analysis of the energy efficiency of intermodal freight trains". *Journal of Rail and Rapid Transit*, Volume 221, pp. 353-364, (2007).